QAL: A Loss for Recall-Precision Balance in 3D Reconstruction

Pranay Meshram Yash Turkar Kartikeya Singh Praveen Raj Masilamani Charuvahan Adhivarahan Karthik Dantu

University at Buffalo, The State University of New York, Buffalo, NY, USA

{pranaywa, yashturk, ksingh35, pmasilam, charuvah, kdantu}@buffalo.edu

Abstract

Volumetric learning underpins many 3D vision tasks such as completion, reconstruction, and mesh generation, yet training objectives still rely on Chamfer Distance (CD) or Earth Mover's Distance (EMD), which fail to balance recall and precision. We propose Quality-Aware Loss (QAL), a drop-in replacement for CD/EMD that combines a coverage-weighted nearest-neighbor term with an uncovered—ground-truth attraction term, explicitly decoupling recall and precision into tunable components.

Across diverse pipelines, QAL achieves consistent coverage gains, improving by an average of +4.3 pts over CD and +2.8 pts over the best alternatives. Though modest in percentage, these improvements reliably recover thin structures and under-represented regions that CD/EMD overlook. Extensive ablations confirm stable performance across hyperparameters and across output resolutions, while full retraining on PCN and ShapeNet demonstrates generalization across datasets and backbones. Moreover, QAL-trained completions yield higher grasp scores under GraspNet evaluation, showing that improved coverage translates directly into more reliable robotic manipulation.

QAL thus offers a principled, interpretable, and practical objective for robust 3D vision and safety-critical robotics pipelines.

1. Introduction

3D perception has become central to applications such as autonomous navigation, infrastructure inspection, dexterous manipulation, and object and scene recognition. This trend is reflected in a growing body of algorithms for 3D object detection and recognition [11, 23, 24, 36, 42], scene segmentation and classification [10, 21, 34, 40], and point cloud completion and estimation [9, 18, 19, 26, 39]. Several factors have enabled this shift from 2D to 3D point-cloud representation: (i) advances in GPUs and mobile hardware [20], (ii) widespread availability of depth sensors

and LiDAR [12], and (iii) deep learning architectures that can capture fine spatial variations and generalize from limited training data. Together, these developments have made large-scale 3D learning feasible and impactful.

3D perception plays a critical role in applications such as autonomous navigation[8], dexterous manipulation[28], and scene reconstruction[5], where reliable geometric understanding is essential. Consider the task of **point cloud completion** [18, 39], where the goal is to recover missing 3D geometry from partial observations. As shown in Fig. 1. when an ECG [18] model is trained with Chamfer Distance (CD), thin or fine structures are often missing (low recall), while other regions exhibit spurious artifacts such as overdense clusters (low precision). This illustrates a broader issue: although widely used, Earth mover's distance (EMD) and CD are scalar distance measures—they average pointto-point errors but fail to capture nuances of the 3D comparisons such as coverage across the whole scene (precision) or the presence/absence of spurious artifacts (recall). In particular, CD tolerates holes and clustering, while EMD enforces one-to-one matching that reduces clustering but often leads to over-smoothed completions where fine details are blurred. Moreover, EMD is computationally expensive, making it impractical at scale and seldom adopted in recent pipelines. Both limitations degrade downstream tasks such as robotic grasping and navigation.

While several variants of CD have been proposed to alleviate these issues, they still treat recall and precision implicitly rather than encoding their balance. Because partial observations are sparse and under-constrained, recovering missing regions (high recall) inevitably increases the risk of spurious predictions (lower precision), making explicit control of this trade-off essential. As illustrated in Fig. 1, even recent variants of CD fail to adequately recover thin structures or suppress spurious artifacts, underscoring the need for a more principled approach. We introduce **Quality-Aware Loss (QAL)**, a differentiable recall–precision objective that explicitly decouples coverage and attraction terms, making the trade-off tunable and interpretable. QAL acts as a *drop-in replacement* in any setting where CD, EMD, or

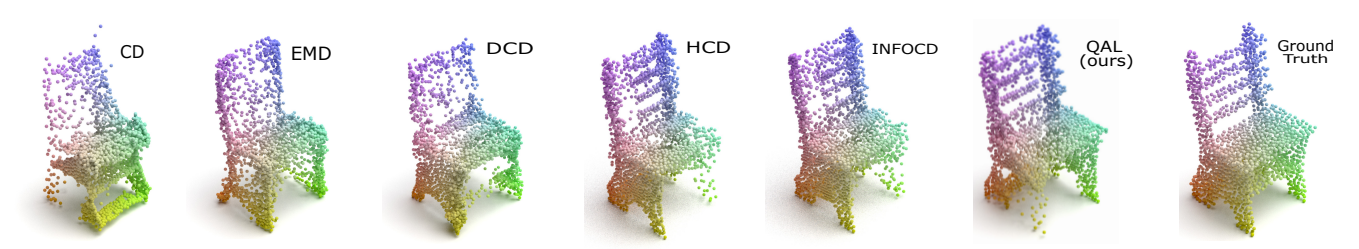


Figure 1. Point cloud completion with ECG [18] on MVP [19]; Input partial clouds are omitted for space; all methods use identical inputs.

their variants are used, aligning optimization with thresholded metrics such as Coverage and F1. Across diverse pipelines—including point-cloud completion, single-view 3D reconstruction, and image-to-mesh generation—QAL consistently improves coverage, with a modest rise in Spurious Points (SP) characteristic of recall-oriented optimization; CD and F1 vary by backbone and dataset but are often comparable or improved. This recall-prioritizing control is particularly valuable for safety-critical robotics tasks, where missing geometry is more costly than mild over-prediction.

The contributions of this work are:

- Quality-Aware Loss (QAL). We introduce QAL, a dropin replacement for Chamfer and Earth Mover's Distance that explicitly balances recall and precision by combining coverage-weighted matching with an uncovered—GT attraction term.
- Comprehensive evaluation. QAL is validated across completion, single-view reconstruction, and mesh generation, and further shown to improve grasp success when integrated into a pre-trained GraspNet model.
- **Practical impact.** We align training with thresholded metrics (Cov@ ϵ , SP@ ϵ) and release efficient GPU implementations and code to enable adoption in 3D vision pipelines.

2. Related Work

Point-set distances and losses. Chamfer Distance (CD) and Earth Mover's Distance (EMD) remain the most widely used objectives for training and evaluating point sets [1, 6]. CD computes bidirectional nearest-neighbor (NN) discrepancies. It is fast and differentiable but sensitive to outliers, tolerates "holes" (low recall), and encourages clustered predictions that miss thin structures. EMD solves a one-to-one assignment (optimal transport) with informative gradients but is computationally heavy (exact solvers scale superlinearly; entropic/Sinkhorn approximations trade bias for speed). Several variants attempt to address these limitations: DCD reweights by local NN density to reduce over-/under-sampling [31]; HCD embeds NN distances in hyperbolic space to preserve fine structures [14]; and InfoCD introduces an information-theoretic margin for discrimination [15]. While effective in some regimes, these methods do not explicitly encode coverage (recall of surface regions) or penalize *spurious predictions* (precision), leaving the recall-precision trade-off implicit. This gap motivates

QAL, which directly incorporates coverage-aware weighting with an uncovered-region attraction signal.

Thresholded coverage and precision metrics. Set coverage and F-score@ τ are widely used to assess completeness and geometric accuracy of reconstructions [1, 25]. We adopt thresholded Coverage (Cov@ τ) as a recall proxy and Spurious Points (SP@ τ) as a precision proxy, aligned with these practices and efficiently implemented on GPU. Unlike raw CD/EMD scores, these thresholded measures explicitly separate recall from precision, making them more interpretable for downstream evaluation. Our work closes the loop by introducing a loss function that is directly aligned with these thresholded metrics, rather than using them only for evaluation.

Point-cloud and single-view 3D learning. Permutationinvariant encoders such as PointNet/PointNet++ [21, 22] introduced set-wise MLP+pool and hierarchical aggregation, while sparse 3D convolutions (Minkowski) enable large-scale voxelized scene processing [2]. Decoders for shape completion and reconstruction typically follow a coarse-to-fine strategy: PCN expands seed points via folding [39], TopNet upsamples with a rooted tree [26], ECG refines predictions through error-correcting graphs [18], and SeedFormer leverages attention for dense surface recovery [41]. Single-view pipelines extend this paradigm to images, ranging from early voxel-based models such as 3D-R2N2 [3, 4] to point-set generators [6] and more recent designs using transformers (LegoFormer) or multi-scale fusion (Pix2Vox/++) [32, 33, 35]. Although these approaches vary in representation and architecture, they almost universally optimize with CD or EMD for supervision, leaving them prone to holes and spurious clusters. This shared reliance makes them natural candidates for OAL, which directly encodes recall and precision while remaining compatible with existing pipelines.

Robotics-driven shape completion. Robotics applications place stricter demands on recall and precision than generic 3D vision tasks. For manipulation and navigation, completing occluded geometry is critical: missing surfaces reduce grasp recall, while spurious points induce false positives. Systems either complete shapes before grasping [27] or plan under uncertainty [16], and are typically evaluated with thresholded surface criteria such as F-score@ τ . Recent efforts such as GraspNet-1Billion [7] emphasize the link between object geometry and grasp success, while learning-based scoring methods [13, 17] show that fine-grained ge-

ometry directly impacts grasp reliability. These findings motivate our evaluation of QAL not only with surface metrics (Cov@ τ /SP@ τ) but also through grasp utility under pre-trained models.

3. Quality Aware Loss Design

In this section, we describe our proposed loss function QAL (Quality-Aware Loss, QAL) and its role in 3D learning. QAL is broadly applicable across volumetric learning tasks and network structures. It captures differences between candidate and reference point clouds along multiple dimensions, enabling faster and more robust learning.

3.1. Motivation

In most volumetric learning applications, Chamfer distance and its derivatives or Earth Movers Distance are the typical loss metrics used. But they optimize only average nearestneighbor distances and therefore agnostic to holes (low recall) and non-uniform densities (low precision), yielding missing parts and spurious clusters. Fig. 1 shows that CDtrained completions omit finer details in the chair despite low mean distance; Hyperbolic CD (HCD) and Info CD (InfoCD) reduce but do not eliminate such omissions (Fig. 6). The primary cause for this is that CD and its variants are blind to missing correspondences: if a ground-truth region has no nearby predictions, the loss does not penalize it, leaving uncovered areas unaddressed. However, several applications such as object recognition, robot localization, 3D tracking etc. require uniform coverage across the scene or object of interest.

QAL addresses these limitations by combining two complementary ideas. First, it emphasizes regions that are under-covered, ensuring that thin or missing structures are recovered. Second, it explicitly attracts predictions toward ground-truth points that would otherwise remain unmatched, closing holes while preserving already accurate regions. The result is a more uniform and complete point set, aligning naturally with thresholded metrics such as Coverage and F1. Fig. 2(a) provides intuition for our proposed Quality-Aware Loss (QAL). The coverage-weighted term (2) reweights nearest-neighbor distances with a soft margin ϵ , down-weighting already well-matched predictions and emphasizing regions that remain under-covered. In parallel, the uncovered-GT attraction term (4) explicitly pulls predictions toward ground-truth points without nearby matches, directly eliminating holes and restoring missing

Together, these two components (orange coverage links and purple attraction links in Fig. 2(a)) encourage recall without disturbing already precise regions, producing point sets that are both more uniform and more complete. This design aligns optimization with commonly used metrics

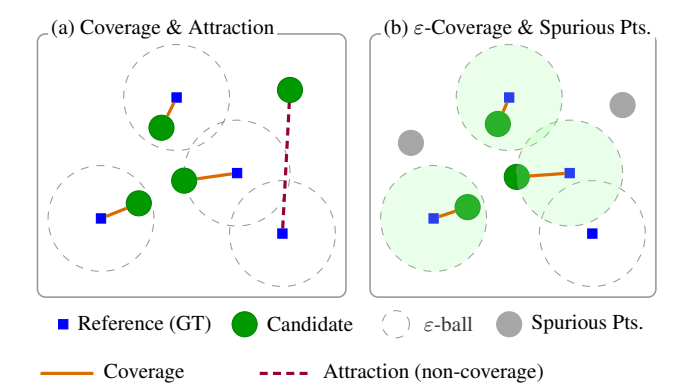


Figure 2. Illustration of QAL and evaluation metrics. (a) QAL components: GT points (blue squares) with ϵ -balls; coverage links (orange) connect GT \rightarrow prediction matches, while attraction links (purple) pull predictions toward uncovered GT regions. (b) Evaluation metrics: predictions inside ϵ -balls are counted toward thresholded coverage, while those outside (gray) are spurious points.

such as Coverage and F1, where missing geometry is typically more harmful than modest over-prediction.

This intuition leads directly to QAL's formulation, which combines coverage-weighted distances with uncovered–GT attraction into a tunable objective that explicitly balances recall and precision.

3.2. Quality-Aware Loss (QAL)

Let $A = \{a_i\}$ be predictions and $B = \{b_j\}$ ground truth. Denote nearest-neighbor distances by $d_a = d(a, B)$ and $d_b = d(b, A)$ for brevity.

Coverage-weighted term. We introduce a soft margin that emphasizes errors beyond a tolerance $\epsilon > 0$:

$$w_{\text{cov}}(d) = 1 - (\sigma(\omega(\epsilon - d)) - 0.5), \quad \omega > 0, \quad (1)$$

where $\sigma(\cdot)$ is the logistic sigmoid. The weighted Chamferstyle loss is:

$$\mathcal{L}_{cov} = \frac{1}{|A|} \sum_{a \in A} w_{cov}(d_a) d_a + \frac{1}{|B|} \sum_{b \in B} w_{cov}(d_b) d_b.$$
 (2)

This term down-weights already precise matches and emphasizes errors outside the ϵ -ball, aligning training with thresholded evaluation metrics such as F-score@1%.

Uncovered-GT attraction. Define the mask

$$m_B(b) = \mathbb{1} [\#\{a \in A : NN_B(a) = b\} = 0],$$
 (3)

which marks ground-truth points b that have no predicted neighbor (i.e., uncovered). Predictions are then attracted toward these regions:

$$\mathcal{L}_{\text{attr}} = \frac{1}{|B|} \sum_{b \in B} m_B(b) \, \sigma(\omega(\epsilon - d_b)) \, d_b. \tag{4}$$

Fig. 2(b) uses a one-way illustration for simplicity; the implemented attraction operates symmetrically on uncovered GT regions.

Algorithm 1 Quality-Aware Loss (QAL)

Require: Predicted set A, ground truth B, tolerance ϵ , sharpness ω , weight $\lambda_{\rm attr}$

- 1: Compute NN distances: $d_a = d(a, B)$ for $a \in A$, $d_b =$ d(b, A) for $b \in B$
- 2: Coverage: $\mathcal{L}_{\text{cov}} = \frac{1}{|A|} \sum_{a} w(d_a) d_a + \frac{1}{|B|} \sum_{b} w(d_b) d_b$, where $w(d) = 1 (\sigma(\omega(\epsilon d)) 0.5)$ 3: Attraction: $\mathcal{L}_{\text{attr}} = \frac{1}{|B|} \sum_{b} m_B(b) \, \sigma(\omega(\epsilon d_b)) d_b$,
- with $m_B(b)=1$ if b unmatched
- 4: Final: $\mathcal{L}_{\mathrm{QAL}} = \mathcal{L}_{\mathrm{cov}} + \lambda_{\mathrm{attr}} \mathcal{L}_{\mathrm{attr}}$
- 5: return \mathcal{L}_{QAL}

Final objective.

$$\mathcal{L}_{\text{QAL}} = \mathcal{L}_{\text{cov}} + \lambda_{\text{attr}} \mathcal{L}_{\text{attr}}, \quad \lambda_{\text{attr}} \ge 0$$
 (5)

where ϵ is the tolerance, ω controls sharpness, and $\lambda_{\rm attr}$ balances coverage and attraction. The overall computation is summarized in Algorithm 1. In practice, ϵ is set to match evaluation tolerance (e.g., 1% of object scale), ω regulates the smoothness of weighting, and $\lambda_{\rm attr}$ is selected via validation ablations (see Sec. 4).

Together, the two terms promote coverage of missing structures while suppressing excessive clustering.

Computational cost. Let N=|A| and M=|B|. Chamfer Distance (two 1-NN passes) runs in O(NM) with bruteforce GPU cdist, or $O((N+M)\log(N+M))$ using kdtrees. QAL shares the same asymptotic cost, adding only O(N+M) for per-point weights and masks [39]. Thus, QAL has CD-like efficiency.

4. Experiments

We evaluate QAL across three complementary settings spanning controlled loss comparisons, large-scale retraining, and task-driven evaluation. First, a micro-benchmark on MVP [19] compares QAL against CD, EMD, and recent variants under identical backbones, isolating the effect of the loss itself. Second, we perform full retraining on PCN [39] and ShapeNet-55 [15] to test generalization across datasets and architectures at higher output resolution. Third, we assess downstream task utility using Grasp-Net [7], where completions trained with QAL are evaluated via grasp quality scores.

For evaluation, we report Chamfer Distance (CD) and F1 as standard metrics, and additionally introduce *Coverage* and Spurious Points to provide a multidimensional assessment of recall-precision balance. We also conduct ablations on hyperparameters and output resolution to study stability. Datasets and Test Pipelines. We evaluate across three representative tasks: point cloud completion, image-to-3D reconstruction, and image-to-mesh reconstruction. MVP [19]

provides multi-view partial point clouds of 16 categories with 62k training and 41k testing pairs. Partial shapes are rendered from ShapeNet CAD models, and ground-truth point clouds are sampled via Poisson Disk Sampling. The PCN benchmark [39] covers 8 ShapeNet categories, where partial inputs are obtained from depth back-projections; we follow the standard train/test split. ShapeNet-55 [15] uses hole/occlusion synthesis under three difficulty levels (S/M/H); we report L2-CD $\times 1e^3$ and F1@ 1% following prior work.

Training Setup. For the MVP micro-benchmark, all networks were trained for 100 epochs with batch size 32 and learning rate 1×10^{-3} . We set $\omega = 10.0$ from ablations, $\epsilon = 0.001$ (1 cm for meter-scale objects), and $\lambda_{\rm attr} = 1.0$. Coverage is reported at $\epsilon = 0.03$, approximately twice the average nearest-neighbor spacing at 2048 points (see Supplementary for details). Nearest-neighbor distance is Euclidean (ℓ_2) in 3D, i.e., $d(x,Y) = \min_{y \in Y} ||x-y||_2$. For fairness, we use official implementations and training protocols, changing only the loss. To highlight coverage under limited capacity, we set the output resolution to 2048 points for MVP. For **PCN** and **ShapeNet-55**, we perform full retraining with the original network settings, including 16K output points, learning rate, batch size, and balance factors. All experiments were run on a workstation with an Intel i9-12900K, 64 GB RAM, and 2 NVIDIA RTX A6000 GPUs.

Evaluation Metrics. In addition to CD, EMD, and F1 [25], we introduce shape-level, thresholded metrics to better expose recall–precision trade-offs. Let d(b, A) be the nearestneighbor distance from $b \in B$ (GT) to A, and d(a, B) analogously. We define:

$$\operatorname{Cov}@\tau = \frac{1}{|B|} \sum_{b \in B} \mathbf{1}[d(b, A) \le \tau],$$

$$\operatorname{SP}@\tau = \frac{1}{|A|} \sum_{a \in A} \mathbf{1}[d(a, B) > \tau].$$
(6)

Here, Cov measures recall of the GT surface and SP measures spurious predictions; Fig. 2(b) provides a visual illustration of the ϵ -ball interpretation used for both metrics. For comparability, we use $\overline{SP} = 1 - SP$ (higher-is-better), and report percentages for both. We also define an aggregate quality score as Quality = $\frac{1}{2}(\text{Cov} + \overline{\text{SP}})$, though in the main text we emphasize per-metric reporting (see Supplementary for grouped-bar visualizations).

4.1. Ablation Studies

We ablate QAL incrementally in three stages (Fig. 3): (1) ϵ sweep with $\omega \approx 10$, $\lambda_{\rm attr} \approx 0.0$ to select ϵ^* by maximizing Cov@ ϵ (ties by minimizing SP@ ϵ , then CD; $\epsilon < 10^{-3}$ gave unstable gradients and diminishing returns), (2) ω sweep at ϵ^{\star} with the same criterion to obtain ω^{\star} , and (3) $\lambda_{\rm attr}$ sweep at (ϵ^*, ω^*) over $\{0, 0.25, 0.5, 1.0, 2.0\}$. Plots show grouped



Figure 3. **QAL hyperparameter ablation.** Each panel shows grouped bars for Coverage (Cov; \uparrow), Spurious Points ($\overline{\mathrm{SP}}$; \uparrow), and Chamfer Distance (CD×10³; \downarrow). Left: ϵ sweep with $\omega \approx 10$, $\lambda_{\mathrm{attr}} \approx 1.0$. Middle: ω sweep at the selected ϵ^* . Right: λ_{attr} sweep at (ϵ^*, ω^*) .

Table 1. Completion Networks trained with CD (L2-CD $\times 1e^3$), HCD, InfoCD and QAL for $\epsilon=0.03$. Cov, \overline{SP} and Quality metrics are scaled as percentages

Method(Network+Loss)	CD↓	<i>F</i> 1 ↑	Cov. ↑	$\overline{SP} \uparrow$	Quality ↑
Wiethod(Network+Loss)	ГСБ↓	I' 1	Cov.	SI	Quanty
PCN [39] + CD	17.4	0.29	59.8	64.0	61.9
PCN + EMD	45.2	0.11	21.1	40.9	31.0
PCN + DCD	17.5	0.29	63.2	62.9	63.1
PCN + HCD	17.5	0.30	59.8	64.3	62.1
PCN + INFOCD	17.2	0.30	62.8	62.5	62.6
PCN + QAL	17.2	0.29	65.9	61.4	63.6
TOP-NET [26] + CD	18.1	0.27	55.2	61.0	58.1
TOP-NET + HCD	18.3	0.27	55.8	60.0	57.9
TOP-NET + INFOCD	18.2	0.27	56.3	60.3	58.3
TOP-NET + QAL	18.3	0.26	59.1	57.7	58.4
ECG [18] + CD	14.0	0.45	66.6	72.1	69.3
ECG + EMD	15.5	0.38	67.0	70.1	68.5
ECG + DCD	14.0	0.45	68.1	71.6	69.8
ECG + HCD	14.0	0.45	66.8	72.4	69.6
ECG + INFOCD	14.0	0.45	67.0	71.2	69.1
ECG + QAL	13.8	0.45	68.9	71.3	70.0
Seedformer [41] + CD	12.3	0.51	73.0	80.8	76.9
Seedformer + INFOCD	14.7	0.41	53.4	85.5	69.5
Seedformer + QAL	12.9	0.47	77.8	74.4	76.1

bars (Cov \uparrow / $\overline{SP}\uparrow$ /CD \downarrow), with CD scaled by 10^3 for readability.

Observations. From Fig. 3, ϵ =0.001 yields the best tradeoff (high Cov, high \overline{SP}), while ϵ =0.1 and ϵ =0.01 underfit the regions; $\epsilon < 10^{-3}$ further leads to unstable gradients and diminishing returns. At ϵ^* , a moderate sharpness $\omega=10$ consistently outperforms $\omega=1$ (weak margin) and ω =100 (overly sharp, slight decrease in \overline{SP}). Finally, at $(\epsilon^{\star}, \omega^{\star})$, increasing λ_{attr} raises Cov but reduces \overline{SP} ; accordingly, CD \times 10³ anti-correlates with \overline{SP} (lower \overline{SP} ⇒ higher CD) since spurious predictions inflate nearestneighbor distances. We therefore pick the Pareto knee at $\lambda_{\rm attr} \in [0.5, 1.0]$, capturing most of the Cov gain while limiting the erosion of \overline{SP} and controlling CD. The exact point can be tuned to application tolerance for false positives. A small Optuna-based search on the lamp category further confirmed that the three hyperparameters are only weakly coupled, exhibiting a broad plateau around $(\epsilon = 10^{-3}, \omega = 10, \lambda_{\text{attr}} \in [0.5, 1.0]).$

4.2. Point cloud completion

PCN [39], TopNet[26], ECG[18] and Seedformer[41] were chosen for evaluation thanks to the availability of code and ease of modification to apply QAL. All models were trained with the same random seed values to ensure invariance to run-to-run deviations. The only modification applied is the change in the loss function to QAL which served as a drop-

Table 2. Comparison on PCN in terms of L1-CD $\times 1e^3$.

Methods	Plane	Cabinet	Car	Chair	Lamp	Couch	Table	Boat	Avg.
TopNet [26]	7.61	13.31	10.90	13.82	14.44	14.78	11.22	11.12	12.15
PCN [39]	5.50	22.70	10.63	8.70	11.00	11.34	11.68	8.59	11.27
InfoCD+PCN	5.07	22.27	10.18	8.26	10.57	10.98	11.23	8.15	10.83
QAL+PCN	5.92	11.09	9.12	11.99	12.70	12.36	9.70	10.42	10.41
FoldingNet [37]	9.49	15.80	12.61	15.55	16.41	15.97	13.65	14.99	14.31
InfoCD+FoldingNe	7.90	12.68	10.83	14.04	14.05	14.56	11.61	11.45	12.14
QAL+FoldingNet	7.62	13.47	11.24	14.00	13.36	14.41	11.75	10.81	12.08
PMP-Net [30]	5.65	11.24	9.64	9.51	6.95	10.83	8.72	7.25	8.73
InfoCD+PMP-Net	4.67	10.09	8.87	8.59	6.38	10.48	7.51	6.75	7.92
QAL+PMP-Net	4.51	9.93	8.69	8.29	6.20	9.86	7.31	6.53	7.66
SeedFormer [41]	3.85	9.05	8.06	7.06	5.21	8.85	6.05	5.85	6.74
QAL+SeedFormer	3.83	8.89	7.80	6.99	5.26	8.72	5.91	5.84	6.65

Table 3. Results on ShapeNet-55 using L2-CD \times 1 e^3 and F1 score.

Methods	Table	Chair	Plane	Car	Sofa	CD-S	CD-M	CD-H Av	/g. F1
PCN [39]	2.13	2.29	1.02	1.85	2.06	1.94	1.96	4.08 2.	66 0.133
QAL + PCN	1.85	2.05	0.93	1.48	1.68	1.78	2.06	3.07 2.	31 0.187
PoinTr [38]	0.81	0.95	0.44	0.91	0.79	0.58	0.88	1.79 1.	09 0.464
QAL+PoinT	0.74	0.87	0.42	0.82	0.72	0.49	0.79	1.64 0.	98 0.52

in replacement. Apart from the change in loss, the networks were trained as intended by their respective authors.

MVP benchmarking and qualitative Coverage, a proxy for recall, increases $(\tau = 0.03m)$. across all backbones when trained with OAL (Tab. 1), with average gains of +4.3 pts (PCN: +6.1, TopNet: +3.9, ECG: +2.3, SeedFormer: +4.8). On PCN (+1.7), TopNet (+0.3), and ECG (+0.7) this also raises the composite Quality, showing that recall gains are achieved with a moderate recall-oriented trade-off; SeedFormer shows a slight Quality drop (-0.8), reflecting the intended recall–precision trade-off. L2-CD shifts are backbone-dependent (lower for PCN/ECG, slightly higher for TopNet/SeedFormer), while F1 remains largely unchanged. Overall, QAL consistently improves recall and often Quality, aligning training with completion behavior desired in practice.

Fig. 4 complements these results with qualitative comparisons for TopNet, PCN, and ECG under CD, HCD, InfoCD, and QAL. SeedFormer is omitted here since we trained it only with CD, InfoCD, and QAL due to its high computational cost, using it mainly for state-of-the-art comparison. Across the other backbones, QAL produces higher coverage with sharper details than CD and HCD. CD often misses regions (e.g., ECG), HCD shows reduced recall (e.g., TopNet), and InfoCD, while competitive, still fails to recover fine structures. Crucially, the slight Coverage gains of QAL are not only reflected quantitatively

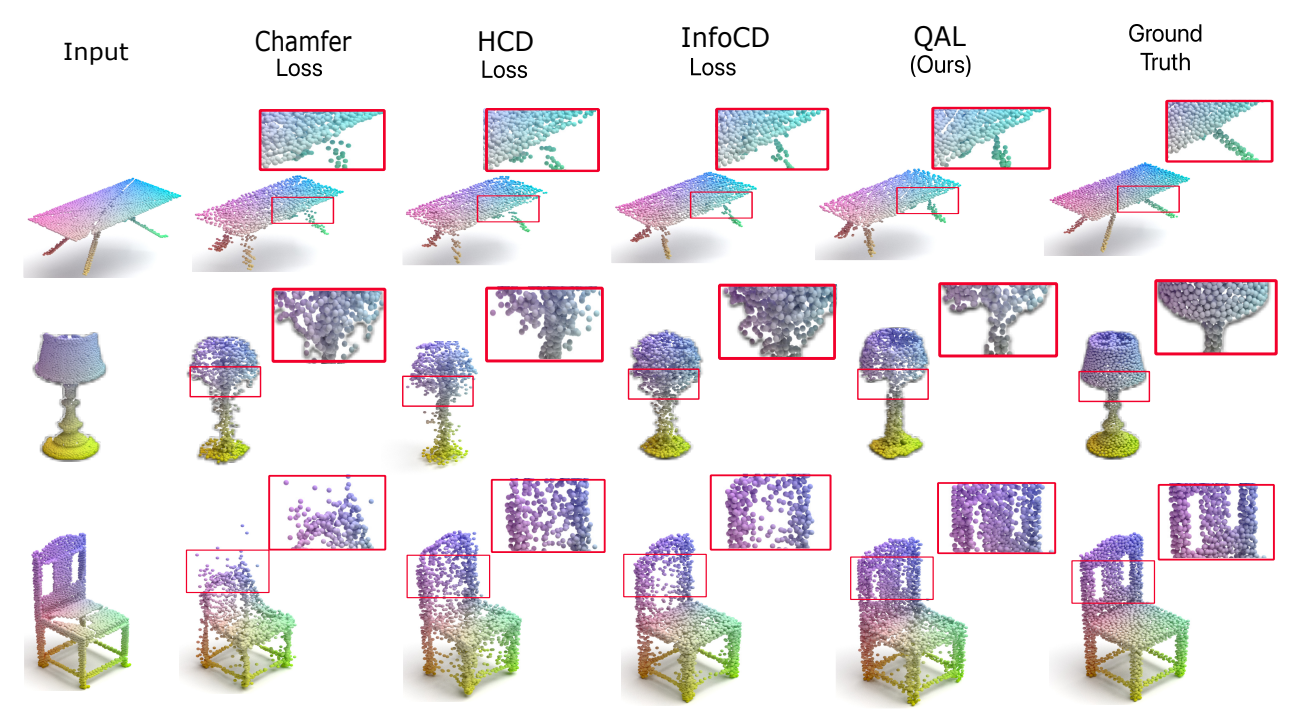


Figure 4. Qualitative results for point cloud completion for samples trained on Topnet, PCN, and ECG (Top to bottom) with four different loss functions CD, HCD, InfoCD, and QAL. The highlighted column with QAL learned more intricate details which are missed in models trained by other loss. These results are on the validation set after 100 epochs of training with $\epsilon = 0.001$, $\omega = 10.0$ and $\lambda_{attr} = 1.0$

but also yield much more impactful qualitative improvements—recovering sharper edges and finer details for more complete reconstructions. These results suggest that the benefits of QAL extend beyond standard geometric metrics. Since sharper edges and improved coverage are especially critical for downstream tasks, we next evaluate how completions from these models influence robotic manipulation performance under a pre-trained GraspNet model (Sec. 4.6).

PCN (L1-CD $\times 1e^3$). QAL improves most where CD tends to accept holes: bulky parts (e.g., Cabinet) and thin appendages. The coverage-weighted term down-weights already-correct pairs inside the ϵ margin, so optimization budget shifts to regions with larger residuals; the uncovered-GT attraction then pulls points into missing areas, preventing the "average-to-the-middle" behavior typical of CD. Coarse-to-fine decoders (PCN, FoldingNet) benefit strongly because their early coarse sets leave sizeable uncovered regions that QAL explicitly targets. Seed-growing models (PMP-Net, SeedFormer) see steadier but smaller gains since they already densify surfaces; QAL still reduces residual and over-concentration by emphasizing uncovered GT. Compared to InfoCD, QAL's uncovered-mask provides a more direct recall signal, which explains its higher gains on categories with large occlusions while remaining competitive elsewhere.

ShapeNet-55 (L2-CD $\times 1e^3$ and F1). On this benchmark, the trends mirror PCN: CD decreases together with higher F1 when training with QAL. This follows from QAL's

alignment with thresholded matching (F-score@ ϵ): emphasizing errors beyond ϵ improves the count of withintolerance matches, which directly lifts F1. Improvements are strongest on the medium/hard splits, where large missing parts are to be completed; here, the attraction term closes gaps that CD leaves unresolved. Architectures that already capture fine detail (e.g., PoinTr) still gain because QAL deprioritizes easy pairs and suppresses spurious clusters just outside the tolerance, converting small geometric fixes into consistent F1 increases.

Across datasets and architectures, QAL consistently lowers Chamfer Distance and raises F1, with the strongest effects on harder splits and occluded/thin structures—aligning with its coverage-first, SP-aware design.

Per-Category Results: Fig. 5 shows a quantitative comparison of performance metrics across various object categories for ECG[18], trained on CD (Chamfer Distance), EMD (Earth Mover's Distance), and QAL. These object categories are grouped into three complexity levels: Easy, Medium, and Hard. This is to underscore performance based on object complexity type.

In Fig. 5(a), the scores represent the L2 norm of the Chamfer Distance (cd_t) . For instance, in the car category, CD scores 4.34, EMD scores 2.98, and QAL scores 2.34. This demonstrates that QAL achieves a score that is significantly lower than CD and EMD, indicating its superior performance. Notably, for lamp, QAL scores 5.50 compared to CD's 17.88 and EMD's 6.20, and for sofa, QAL has a score

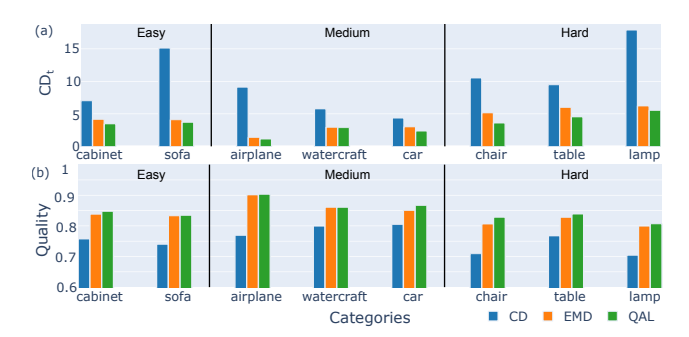


Figure 5. Per-category metric scores comparison for ECG model trained with three loss functions: CD, EMD, and QAL. Metric comparison for (a) CD_t and (b) Quality: equally weighted average of Cov, \overline{SP} . The categories are divided based on the complexity of the object structure.

of 3.68 against CD's 15.11 and EMD's 4.07. These scores indicate a consistent improvement in CD_t metric value if the model is trained with QAL.

The plot in Fig. 5(b) depicts Quality, computed as the average of the metrics: Cov, \overline{SP} . Here, higher scores indicate better performance. Again, QAL consistently attains the highest scores. For example, in car, it scores 0.87, outperforming the next best scores by EMD (0.85), and while for chair (QAL 0.83) we can see a substantial improvement from CD (0.71) while also outperforming EMD (0.81). These results underscore the effectiveness of QAL in not only minimizing cd_t but also in enhancing the overall quality of the models, as measured by Quality metrics.

Networks trained using QAL produce point clouds with higher coverage and fewer spurious points compared to CD and EMD-based loss functions. This means that networks trained with QAL are more effective at not only capturing local structure and point distribution but also in reducing SP that may cause the resulting shape to contain misaligned points and noise. This is particularly important in applications where the fidelity of the reconstructed shape to the true structure is critical. Moreover, the quality score, which is an aggregate measure of the models' performance (COV, \overline{SP}) , is highest for models trained with QAL. This captures the general superiority of QAL-trained models over those trained with CD and EMD loss functions, confirming that QAL is a superior loss function for training point cloud neural networks.

4.3. Image to 3D Reconstruction

Point Set Generation Network [6] is a pioneer in the single image to 3D reconstruction domain. We use PSG to evaluate the performance of QAL by replacing CD and EMD loss used in PSG with QAL. Tab. 4 shows QAL coverage improvements when compared with CD and EMD. As PSG is only trained for the 1000 epochs, the resolution doesn't increase, resulting in low resolution. Having said that, Fig. 1 and Fig. 6 show that qualitatively QAL produces point clouds with high coverage and a much better

Table 4. Image to 3D points Generation and Mesh generation with QAL Loss (Validation ϵ =0.09m, L1-CD \times 1 e^3). Quality metrics are percentages.

Network	Loss	$CD_t \downarrow$	$EMD\downarrow$	$F1\uparrow $	$Cov. \uparrow$	$\overline{SP}\uparrow$	$Quality \uparrow$
P2M [29]	CD QAL	0.0044 0.0049	2726 1087	0.80 0.83	78 86	77 82	78 86
PSG [6]	CD EMD QAL	0.004 0.011 0.002	5586 3548 2496	0.68 0.78 0.83	49 37 72	48 52 60	50 51 62

Table 5. PCN with QAL on the lamp category at different output resolutions. QAL maintains strong coverage and quality across densities, indicating robustness to output point count even on a hard class with thin structures.(Validation ϵ =0.03, L1-CD \times 1 e^3)

Resolution	l Loss	$CD_t \downarrow$	$F1\uparrow$	$ Cov.\uparrow$	$\overline{SP} \uparrow$	$Quality \uparrow$
2048	EMD	14.7	0.11	20.5	28.1	24.3
	CD	2.6	0.18	40.4	46.0	43.2
	QAL	2.3	0.25	49.7	45.5	47.6
4096	EMD	15.9	0.14	20.5	29.0	27.3
	CD	2.5	0.25	50.0	47.0	48.5
	CD QAL	2.1	0.32	57.5	46.5	52.0
8192	EMD	18.0	0.17	28.0	34.3	31.1
	CD	2.4	0.31	57.0	46.3	51.7
	QAL	2.0	0.38	63.0	46.5	54.8

appearance. Through these results, we show that Quality score, with the even weighting scheme, although meaningful for one application like Sec. 4.2 is inadequate for this application. From the given table, we observe a drastic increase in the coverage when compared to CD and EMD. Since PSG considers a set of fixed-length random vectors as an input space, the resolution and \overline{SP} in the case of CD and EMD increases. However, the coverage metric is significantly low, causing a qualitative degradation where the object clearly appears skewed or sparse.

4.4. Image to Mesh

A third application, Pixel2Mesh [29] is used to further scrutinize QAL. Pixel2Mesh is a well-known benchmark for a single image to 3D mesh reconstruction, which uses CD loss with three other mesh-specific losses as their loss function. In the interest of consistency, we swap CD loss with QAL and use the same ShapeNet dataset as the authors. Tab. 4 shows that QAL performs competitively.

4.5. Effect of Resolution

Tab. 5 reports PCN trained with QAL at different output resolutions (2048, 4096, 8192 points), using the **lamp category** as it is considered one of the most challenging classes due to its thin structures and fine details. Performance remains consistent across densities, showing that QAL generalizes robustly to varying output point counts without requiring re-tuning.

4.6. Impact of Completion on Grasp Utility

Beyond geometric metrics, we investigate how improved completion and coverage affect the utility of reconstructed

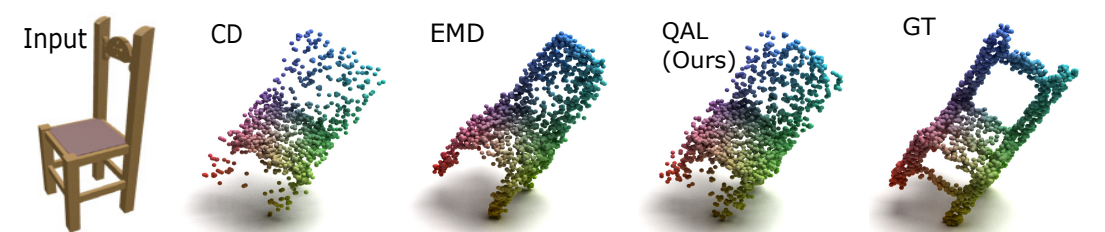


Figure 6. Qualitative results from training PSG for 1000 epochs using CD, EMD, and QAL loss.

Table 6. ECG model predictions evaluated for grasp score and number of grasps across different loss functions on the GraspNet-1Billion dataset [7]. Best mean score is highlighted in bold.

Loss	Grasp Score (Mean \pm Std)	Num Grasps
CD	0.5379 ± 0.3456	85.54
EMD	0.5239 ± 0.3948	108.77
HCD	0.5264 ± 0.3444	82.19
DCD	0.5324 ± 0.3484	87.98
INFOCD	0.5353 ± 0.3478	86.10
QAL	0.5417 ± 0.3461	90.48

point clouds for manipulation. We evaluate ECG models trained on the MVP dataset with all the losses considered in Tab. 1. To focus on the effect of high-coverage completions, we sample the top 1500 QAL reconstructions ranked by $\text{Cov}@\epsilon$ and evaluate them, along with corresponding predictions from other baselines, using a pre-trained GraspNet model [7]. The model predicts candidate grasps and assigns a grasp quality score, providing a task-driven evaluation: if completions better preserve object geometry, they should yield higher grasp scores and enable more feasible grasps.

Tab. 6 reports the results across six losses. QAL achieves the **highest average grasp score** (0.5417 \pm 0.3461), while EMD yields the largest number of feasible grasps (108.8 on average). These results highlight a trade-off: coverage-oriented objectives like QAL lead to higher-quality grasps, whereas EMD emphasizes grasp diversity. Overall, the findings validate that completion quality and coverage directly enhance the downstream utility of point clouds for grasp manipulation.

5. Discussion

What QAL optimizes. QAL makes the recall–precision trade-off explicit: its coverage-weighted term emphasizes errors beyond a tolerance ϵ (precision proxy), while the uncovered–GT attraction activates where recall is missing. This aligns training with thresholded metrics such as Coverage, Spurious Points, and F1, providing a more diagnostic view of performance than CD or EMD alone. Across backbones, QAL consistently improves Coverage, with the effect on spurious points moderated by $\lambda_{\rm attr}$.

Quantitative vs. qualitative impact. Although average Coverage gains over CD and its variants appear modest (+3–4 pts), they correspond to meaningful improvements in geometry. As illustrated in Fig. 4, even small increases in coverage restore thin structures and sharper edges that CD-based models typically miss. CD and F1, while standard, often provide ambiguous signals—CD may

differ even when recall/precision are unchanged, and F1 can remain flat despite recovered details—whereas Cov and SP capture these improvements more faithfully. Further evaluation in the supplementary (see Sec. J) confirms this trend, showing that QAL better preserves detail and suppresses artifacts even in simple reconstruction settings. This explains why QAL-trained completions also yield higher grasp scores in GraspNet evaluation: improved completeness provides more reliable surfaces for downstream use.

Practicality and limitations. Ablations show that QAL performs robustly across a range of hyperparameters and output resolutions, with $\epsilon = 10^{-3}$, $\omega = 10$, and $\lambda_{\rm attr} \in [0.5, 1.0]$ serving as stable defaults. Nonetheless, highly occluded or ambiguous shapes remain challenging, where the attraction term may introduce mild overprediction (see Fig. 7 in the supplementary material). These cases suggest future directions such as incorporating stronger shape priors or adaptive scheduling of ϵ and $\lambda_{\rm attr}$ to further refine the recall–precision balance. Finally, our grasp evaluation relies on GraspNet's simulated scoring rather than physical grasp trials, so confirming these gains on real hardware remains future work.

6. Conclusion

We introduced QAL, a differentiable loss that decouples coverage and attraction terms to explicitly balance recall and precision. Across four completion backbones, QAL improves Coverage by an average of +4.3 pts, consistently recovering thin structures and details missed by CD- and EMD-based models. We further demonstrate generalization beyond point cloud completion, showing consistent improvements in single-image 3D reconstruction and imageto-mesh generation, as well as higher grasp scores under GraspNet evaluation. As a simple, interpretable dropin replacement wherever CD/EMD or their variants are used, QAL provides a principled way to align training with thresholded metrics such as Coverage and F1. Its recalloriented formulation makes it broadly applicable across 3D vision pipelines, with potential benefits for large-scale reconstruction and safety-critical domains where missing geometry is particularly costly.

References

[1] Panos Achlioptas, Olga Diamanti, Ioannis Mitliagkas, and Leonidas Guibas. Learning representations and generative

- models for 3d point clouds. In *International conference on machine learning*, pages 40–49. PMLR, 2018. 2
- [2] Christopher Choy, Jun Young Gwak, and Silvio Savarese. 4d spatio-temporal convnets: Minkowski convolutional neural networks, 2019. 2
- [3] Christopher B Choy, Danfei Xu, Jun Young Gwak, Kevin Chen, and Silvio Savarese. 3d-r2n2: A unified approach for single and multi-view 3d object reconstruction. In Computer Vision–ECCV 2016: 14th European Conference, Amsterdam, The Netherlands, October 11-14, 2016, Proceedings, Part VIII 14, pages 628–644. Springer, 2016. 2
- [4] Christopher B. Choy, Danfei Xu, JunYoung Gwak, Kevin Chen, and Silvio Savarese. 3D-R2N2: A Unified Approach for Single and Multi-view 3D Object Reconstruction, 2016. arXiv:1604.00449 [cs]. 2
- [5] Tao Chu, Pan Zhang, Qiong Liu, and Jiaqi Wang. Buol: A bottom-up framework with occupancy-aware lifting for panoptic 3d scene reconstruction from a single image. In Proceedings of the IEEE/CVF Conference on Computer Vision and Pattern Recognition (CVPR), pages 4937–4946, 2023. 1
- [6] Haoqiang Fan, Hao Su, and Leonidas J Guibas. A point set generation network for 3d object reconstruction from a single image. In *Proceedings of the IEEE conference on computer* vision and pattern recognition, pages 605–613, 2017. 2, 7
- [7] Hao-Shu Fang, Chenxi Wang, Minghao Gou, and Cewu Lu. Graspnet-1billion: A large-scale benchmark for general object grasping. In *Proceedings of the IEEE/CVF Conference on Computer Vision and Pattern Recognition(CVPR)*, pages 11444–11453, 2020. 2, 4, 8
- [8] Yihan Hu, Jiazhi Yang, Li Chen, Keyu Li, Chonghao Sima, Xizhou Zhu, Siqi Chai, Senyao Du, Tianwei Lin, Wenhai Wang, Lewei Lu, Xiaosong Jia, Qiang Liu, Jifeng Dai, Yu Qiao, and Hongyang Li. Planning-oriented autonomous driving. In Proceedings of the IEEE/CVF Conference on Computer Vision and Pattern Recognition (CVPR), pages 17853– 17862, 2023. 1
- [9] Zitian Huang, Yikuan Yu, Jiawen Xu, Feng Ni, and Xinyi Le. Pf-net: Point fractal network for 3d point cloud completion. In Proceedings of the IEEE/CVF Conference on Computer Vision and Pattern Recognition (CVPR), 2020. 1
- [10] Xin Lai, Jianhui Liu, Li Jiang, Liwei Wang, Hengshuang Zhao, Shu Liu, Xiaojuan Qi, and Jiaya Jia. Stratified transformer for 3d point cloud segmentation. In *Proceedings of* the IEEE/CVF Conference on Computer Vision and Pattern Recognition, pages 8500–8509, 2022. 1
- [11] Alex H. Lang, Sourabh Vora, Holger Caesar, Lubing Zhou, Jiong Yang, and Oscar Beijbom. Pointpillars: Fast encoders for object detection from point clouds. In *Proceedings of* the IEEE/CVF Conference on Computer Vision and Pattern Recognition (CVPR), 2019. 1
- [12] Nanxi Li, Chong Pei Ho, Jin Xue, Leh Woon Lim, Guanyu Chen, Yuan Hsing Fu, and Lennon Yao Ting Lee. A Progress Review on Solid-State LiDAR and Nanophotonics-Based Li-DAR Sensors. *Laser & Photonics Reviews*, 16(11):2100511, 2022.
- [13] Hongzhuo Liang, Xiaojian Ma, Shuang Li, Michael Görner, Song Tang, Bin Fang, Fuchun Sun, and Jianwei Zhang.

- Pointnetgpd: Detecting grasp configurations from point sets. In 2019 International Conference on Robotics and Automation (ICRA), pages 3629–3635. IEEE, 2019. 2
- [14] Fangzhou Lin, Yun Yue, Songlin Hou, Xuechu Yu, Yajun Xu, Kazunori D Yamada, and Ziming Zhang. Hyperbolic chamfer distance for point cloud completion. In *Proceedings of* the IEEE/CVF International Conference on Computer Vision (ICCV), pages 14595–14606, 2023. 2
- [15] Fangzhou Lin, Yun Yue, Ziming Zhang, Songlin Hou, Kazunori Yamada, Vijaya Kolachalama, and Venkatesh Saligrama. Infocd: A contrastive chamfer distance loss for point cloud completion. Advances in Neural Information Processing Systems, 36:76960–76973, 2023. 2, 4
- [16] Jens Lundell, Francesco Verdoja, and Ville Kyrki. Beyond top-grasps through scene completion. In 2020 IEEE International Conference on Robotics and Automation (ICRA), pages 545–551. IEEE, 2020. 2
- [17] Douglas Morrison, Peter Corke, and Jürgen Leitner. Learning robust, real-time, reactive robotic grasping. *The International journal of robotics research*, 39(2-3):183–201, 2020.
- [18] Liang Pan. ECG: Edge-aware Point Cloud Completion with Graph Convolution. *IEEE Robotics and Automation Letters*, 5(3):4392–4398, 2020. 1, 2, 5, 6, 11, 12
- [19] Liang Pan, Xinyi Chen, Zhongang Cai, Junzhe Zhang, Haiyu Zhao, Shuai Yi, and Ziwei Liu. Variational relational point completion network. In *Proceedings of the IEEE/CVF conference on computer vision and pattern recognition*, pages 8524–8533, 2021. 1, 2, 4, 11, 12
- [20] Mohit Pandey, Michael Fernández, Francesco Gentile, Olexandr Isayev, Alexander Tropsha, Abraham C. Stern, and Artem Cherkasov. The transformational role of GPU computing and deep learning in drug discovery. *Nat. Mach. In*tell., 4(3):211–221, 2022. 1
- [21] Charles R. Qi, Li Yi, Hao Su, and Leonidas J. Guibas. Point-Net++: Deep Hierarchical Feature Learning on Point Sets in a Metric Space, 2017. 1, 2
- [22] Charles R. Qi, Li Yi, Hao Su, and Leonidas J. Guibas. Point-Net++: Deep Hierarchical Feature Learning on Point Sets in a Metric Space, 2017. arXiv:1706.02413 [cs]. 2
- [23] Charles R. Qi, Or Litany, Kaiming He, and Leonidas J. Guibas. Deep hough voting for 3d object detection in point clouds. In 2019 IEEE/CVF International Conference on Computer Vision, ICCV 2019, Seoul, Korea (South), October 27 November 2, 2019, pages 9276–9285. IEEE, 2019.
- [24] Shaoshuai Shi, Xiaogang Wang, and Hongsheng Li. Pointrcnn: 3d object proposal generation and detection from point cloud. In Proceedings of the IEEE/CVF Conference on Computer Vision and Pattern Recognition (CVPR), 2019. 1
- [25] Maxim Tatarchenko, Stephan R. Richter, Rene Ranftl, Zhuwen Li, Vladlen Koltun, and Thomas Brox. What do single-view 3d reconstruction networks learn? In Proceedings of the IEEE/CVF Conference on Computer Vision and Pattern Recognition (CVPR), 2019. 2, 4
- [26] Lyne P. Tchapmi, Vineet Kosaraju, Hamid Rezatofighi, Ian Reid, and Silvio Savarese. TopNet: Structural Point Cloud

- Decoder. In 2019 IEEE/CVF Conference on Computer Vision and Pattern Recognition (CVPR), pages 383–392, Long Beach, CA, USA, 2019. IEEE. 1, 2, 5
- [27] Jacob Varley, Chad DeChant, Adam Richardson, Joaquín Ruales, and Peter Allen. Shape completion enabled robotic grasping. In 2017 IEEE/RSJ international conference on intelligent robots and systems (IROS), pages 2442–2447. IEEE, 2017. 2
- [28] Weikang Wan, Haoran Geng, Yun Liu, Zikang Shan, Yaodong Yang, Li Yi, and He Wang. Unidexgrasp++: Improving dexterous grasping policy learning via geometryaware curriculum and iterative generalist-specialist learning. In *Proceedings of the IEEE/CVF International Conference* on Computer Vision (ICCV), pages 3891–3902, 2023. 1
- [29] Nanyang Wang, Yinda Zhang, Zhuwen Li, Yanwei Fu, Wei Liu, and Yu-Gang Jiang. Pixel2mesh: Generating 3d mesh models from single rgb images. In *Proceedings of the Euro*pean Conference on Computer Vision (ECCV), 2018. 7
- [30] Xin Wen, Peng Xiang, Zhizhong Han, Yan-Pei Cao, Pengfei Wan, Wen Zheng, and Yu-Shen Liu. Pmp-net: Point cloud completion by learning multi-step point moving paths. In *Proceedings of the IEEE/CVF conference on computer vision and pattern recognition*, pages 7443–7452, 2021. 5
- [31] Tong Wu, Liang Pan, Junzhe Zhang, Tai Wang, Ziwei Liu, and Dahua Lin. Density-aware Chamfer Distance as a Comprehensive Metric for Point Cloud Completion, 2021. arXiv:2111.12702 [cs]. 2
- [32] Haozhe Xie, Hongxun Yao, Xiaoshuai Sun, Shangchen Zhou, and Shengping Zhang. Pix2vox: Context-aware 3d reconstruction from single and multi-view images. In Proceedings of the IEEE/CVF international conference on computer vision, pages 2690–2698, 2019. 2
- [33] Haozhe Xie, Hongxun Yao, Shengping Zhang, Shangchen Zhou, and Wenxiu Sun. Pix2vox++: Multi-scale context-aware 3d object reconstruction from single and multiple images. *International Journal of Computer Vision*, 128(12): 2919–2935, 2020. 2
- [34] Chenfeng Xu, Bichen Wu, Zining Wang, Wei Zhan, Peter Vajda, Kurt Keutzer, and Masayoshi Tomizuka. Squeezesegv3: Spatially-adaptive convolution for efficient pointcloud segmentation. In European Conference on Computer Vision, pages 1–19. Springer, 2020. 1
- [35] Farid Yagubbayli, Yida Wang, Alessio Tonioni, and Federico Tombari. Legoformer: Transformers for block-by-block multi-view 3d reconstruction. arXiv preprint arXiv:2106.12102, 2021. 2
- [36] Bin Yang, Wenjie Luo, and Raquel Urtasun. Pixor: Realtime 3d object detection from point clouds. In Proceedings of the IEEE Conference on Computer Vision and Pattern Recognition (CVPR), 2018. 1
- [37] Yaoqing Yang, Chen Feng, Yiru Shen, and Dong Tian. Foldingnet: Point cloud auto-encoder via deep grid deformation. In *Proceedings of the IEEE conference on computer vision and pattern recognition*, pages 206–215, 2018. 5
- [38] Xumin Yu, Yongming Rao, Ziyi Wang, Zuyan Liu, Jiwen Lu, and Jie Zhou. Pointr: Diverse point cloud completion with geometry-aware transformers. In *Proceedings of*

- the IEEE/CVF international conference on computer vision, pages 12498–12507, 2021. 5
- [39] Wentao Yuan, Tejas Khot, David Held, Christoph Mertz, and Martial Hebert. PCN: Point Completion Network. In 2018 International Conference on 3D Vision (3DV), pages 728– 737, Verona, 2018. IEEE. 1, 2, 4, 5
- [40] Hengshuang Zhao, Li Jiang, Jiaya Jia, Philip H.S. Torr, and Vladlen Koltun. Point transformer. In *Proceedings of the IEEE/CVF International Conference on Computer Vision* (ICCV), pages 16259–16268, 2021. 1
- [41] Haoran Zhou, Yun Cao, Wenqing Chu, Junwei Zhu, Tong Lu, Ying Tai, and Chengjie Wang. Seedformer: Patch seeds based point cloud completion with upsample transformer. arXiv preprint arXiv:2207.10315, 2022. 2, 5
- [42] Yin Zhou and Oncel Tuzel. Voxelnet: End-to-end learning for point cloud based 3d object detection. In *Proceedings* of the IEEE Conference on Computer Vision and Pattern Recognition (CVPR), 2018. 1

G. QAL: Supplementary Material

We provide extended qualitative comparisons on the MVP dataset [19] using the ECG [18] backbone trained with different loss functions. Figure 8 shows representative success cases. Across diverse object categories, QAL yields completions with *fewer spurious points*, better preservation of *thin structures* such as chair legs and lamp posts, and sharper recovery of *fine geometric details* compared to CD, EMD, DCD, HCD, and InfoCD. These improvements demonstrate QAL's ability to balance recall and precision, producing reconstructions that are both complete and clean.

To complement these strengths, Figure 7 presents challenging failure cases. While QAL generally outperforms existing losses, objects with highly irregular or ambiguous geometry remain difficult: elongated parts may still be under-reconstructed, flat surfaces can appear distorted, and spurious points may emerge under severe occlusion. These examples highlight open challenges in reliably capturing fine details from severely incomplete observations and suggest promising directions for future work on stronger priors and shape reasoning.

H. Per-Category Coverage Analysis

To provide a more detailed view of reconstruction quality, we report **per-category coverage** across all models and loss functions in Table 7. While the main paper highlights average performance, these results reveal finer trends within individual object categories of the MVP dataset.

Several observations emerge. First, **QAL consistently** achieves the highest coverage across most categories and models, often improving upon CD, HCD, and InfoCD. For instance, on *airplane*, *cabinet*, and *table* objects, QAL provides clear gains over both CD and InfoCD. Second, al-

though EMD enforces one-to-one correspondences, its coverage remains markedly lower across categories, underscoring its tendency to produce over-smoothed reconstructions. Finally, categories with thin or fine-grained structures such as *lamp* and *chair* show the greatest benefit from QAL, where balancing recall and precision is critical to capturing delicate geometric details.

These category-level results complement the aggregate analysis and further validate the robustness of QAL: it improves completeness of reconstructions without sacrificing precision, even on challenging object classes.

I. Evaluation Protocol and Trade-off Analysis

Choice of ϵ for Coverage Evaluation We report coverage at a fixed threshold of $\epsilon=0.03$. This value was selected based on the average nearest-neighbor spacing in MVP samples at 2048 points, which is approximately 0.0156. Setting ϵ to twice this mean spacing provides a strict enough tolerance to penalize missing thin structures, while remaining flexible enough to ignore minor surface noise or small alignment discrepancies. Empirically, thresholds lower than 0.02 excessively penalized completions for surface noise, while thresholds above 0.05 blurred differences between methods.

Reporting Trade-offs Recall-oriented training with QAL naturally induces a trade-off between recall and precision. To highlight this, we present grouped bar plots in our ablations, showing Cov (\uparrow), the complement of spurious points \overline{SP} (\uparrow), and Chamfer Distance (CD; \downarrow) side-by-side for each hyperparameter setting. This visualization makes trade-offs explicit without collapsing into a single score. While we report an aggregate quality metric in the main paper for completeness, we emphasize that per-metric reporting provides clearer insight into how QAL balances recall and precision.

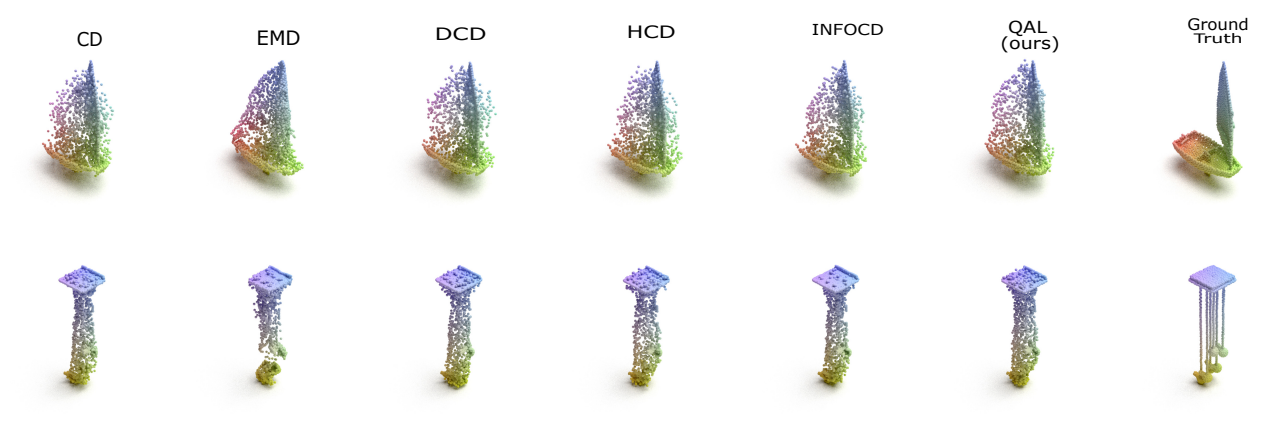


Figure 7. Failure cases of point cloud completion on challenging MVP samples [19]. Each row shows an input partial point cloud and completions generated by ECG [18] trained with CD, EMD, DCD, HCD, InfoCD, and our proposed QAL, followed by the ground truth. While QAL generally outperforms existing losses, certain instances with complex geometry remain difficult: thin or elongated parts may be under-reconstructed, and spurious points can still appear around highly ambiguous regions. These examples highlight open challenges in reliably capturing fine details under severe incompleteness. Input partial clouds are omitted for space; all methods use identical inputs.

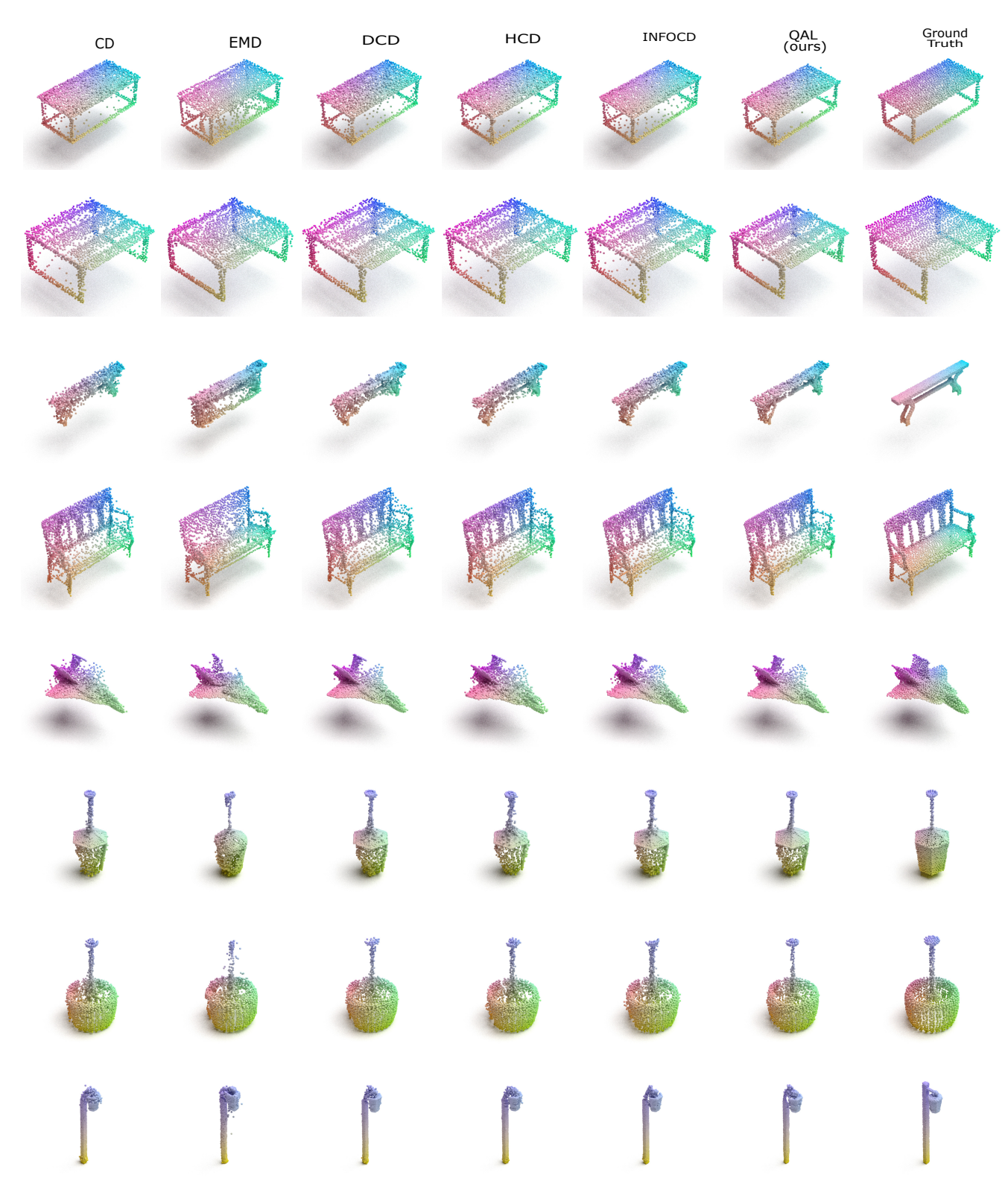


Figure 8. Qualitative comparisons of point cloud completion across 8 representative object categories from the MVP dataset [19]. Each row shows an input partial point cloud and completions generated by ECG [18] trained with CD, EMD, DCD, HCD, InfoCD, and our proposed QAL, followed by the ground truth. QAL consistently recovers thin structures (e.g., chair legs, lamp posts) and suppresses spurious artifacts, producing reconstructions that are both more complete and geometrically faithful compared to existing losses. Input partial clouds are omitted for space; all methods use identical inputs.

Table 7. Per-category coverage (%) across models and loss functions on the MVP dataset. QAL consistently achieves the highest coverage, with best results highlighted in bold.(Validation ϵ =0.03)

Model	Loss	Airplane	Cabinet	Car	Chair	Lamp	Sofa	Table	Boat	Average
	CD	77.0	55.3	62.3	50.9	56.1	53.3	56.4	67.1	59.8
	EMD	34.5	13.2	20.8	17.2	11.0	27.0	30.7	14.2	21.1
PCN	DCD	78.5	61.2	67.0	54.0	56.6	58.7	59.6	70.4	63.2
rcn	HCD	77.0	56.0	63.1	50.3	54.3	53.3	57.3	67.3	59.8
	InfoCD	77.6	58.2	65.9	55.1	59.3	57.1	58.9	70.1	62.8
	QAL	79.7	61.1	68.4	58.1	62.2	60.7	62.6	74.5	65.9
	CD	75.0	49.7	57.0	45.6	49.8	47.1	52.0	65.7	55.2
TOPNET	HCD	75.5	48.7	56.0	45.9	53.0	47.8	52.4	67.0	55.8
TOFNET	InfoCD	74.9	49.7	57.9	46.0	55.2	47.4	52.8	66.2	56.3
	QAL	77.7	51.1	60.0	49.5	57.9	50.7	55.3	70.4	59.1
	CD	85.7	56.0	60.2	61.4	71.5	56.7	68.0	73.2	66.6
	EMD	83.1	59.5	61.5	61.1	71.2	59.8	66.9	72.8	67.0
ECG	DCD	86.0	58.6	62.8	62.7	72.1	58.6	69.8	74.5	68.1
ECG	HCD	85.4	57.0	60.3	61.7	71.5	56.9	68.7	72.8	66.8
	InfoCD	85.3	57.0	61.8	62.1	71.3	57.7	66.7	74.0	67.0
	QAL	87.2	59.3	63.1	63.4	73.3	59.2	70.0	75.8	68.9
Seedformer	CD	86.1	67.4	66.4	69.4	77.8	66.6	72.9	77.7	73.0
	InfoCD	76.7	38.4	40.1	50.7	64.0	41.5	56.9	58.8	53.4
	QAL	89.5	70.0	73.5	73.8	81.1	72.4	77.4	85.1	77.8

J. Effect of Loss on Reconstruction.

Using the same trained models from Section 4.2 (Table 1), we further evaluate reconstruction performance when ground-truth point clouds are provided as input on the MVP dataset (1200 samples). This controlled setting removes the challenge of inferring missing regions and highlights how the choice of loss function alone shapes the fidelity of the reconstructed geometry. Table 8 shows that while CD and F1 remain standard, they often provide incomplete or even misleading signals. For example, in PCN, QAL improves Coverage by +4.5 pts over CD (65.3 vs. 60.8) while CD and F1 remain nearly unchanged, masking the recovery of fine details. In TOPNet, CD and F1 suggest negligible differences across losses, yet Coverage and Quality reveal that QAL yields denser and more uniform reconstructions (+4.3 pts Coverage over CD). In ECG, HCD and QAL achieve near-identical Cov (91.6) and \overline{SP} (\sim 81), yet CD differs (6.0 vs. 5.8), illustrating that CD alone can produce misleading signals even when recall and precision are effectively the same. Finally, in SeedFormer, F1 stays nearly flat across CD, InfoCD, and QAL (0.62–0.66), while Coverage rises from 87.8 (CD) to 88.3 (QAL), and Quality remains competitive despite InfoCD reporting the lowest CD.

This confirms that CD and F1 alone cannot capture the nuanced trade-offs between recall and precision. To complement these quantitative results, we also include 3–4 representative visualizations per model (Figs. 9 to 12). These examples qualitatively confirm the same trends: QAL consistently recovers sharper structures and reduces holes relative to CD/EMD, while avoiding the spurious clusters sometimes induced by InfoCD or HCD. Such visualizations rein-

Table 8. Completion Networks trained with CD (L2-CD $\times 1e^3$), HCD, InfoCD and QAL for $\epsilon=0.03$. Cov, \overline{SP} and Quality metrics are scaled as percentages.

Method (Network+Loss)	CD (\dagger)	F1 (†)	Cov. (†)	$\overline{SP}\left(\uparrow\right)$	Quality (†)
PCN + CD	17.0	0.30	60.8	64.6	62.7
PCN + EMD	44.0	0.11	21.9	41.3	31.6
PCN + HCD	17.2	0.31	60.4	64.5	62.4
PCN + INFO	16.9	0.30	63.6	62.7	63.2
PCN + QAL	16.9	0.31	64.8	63.1	64.0
TOPNET + CD	17.7	0.28	56.2	60.9	58.6
TOPNET + HCD	17.8	0.28	56.8	60.1	58.4
TOPNET + INFO	17.7	0.28	57.4	60.3	58.8
TOPNET + QAL	17.8	0.27	60.5	57.9	59.2
ECG + CD	6.2	0.82	90.9	80.6	85.8
ECG + EMD	11.8	0.49	82.8	77.3	80.0
ECG + DCD	6.1	0.80	91.0	79.9	85.4
ECG + HCD	6.0	0.82	91.6	81.0	86.3
ECG + INFO	6.6	0.81	89.6	79.7	84.6
ECG + QAL	5.8	0.81	91.6	80.9	86.2
SEEDFORMER + CD	9.4	0.62	87.8	87.8	87.8
SEEDFORMER + INFO	5.9	0.65	75.1	95.8	85.4
SEEDFORMER + QAL	8.4	0.66	88.3	87.1	87.7

force that the geometric advantages highlighted by Cov and \overline{SP} are clearly visible in the reconstructions.

These cases highlight that CD favors small average distances, while F1 is threshold-sensitive and may improve even if reconstructions cluster unnaturally, leading to contradictory interpretations. By contrast, the additional dimensions introduced here—Cov and $\overline{\rm SP}$ —capture complementary geometric aspects: whether fine details are covered and whether spurious points are suppressed. Together, they resolve the ambiguity of CD/F1 and provide a more faithful picture of reconstruction quality, confirming that QAL not only benefits partial-to-complete completion but also enhances detail preservation in autoencoding scenarios.

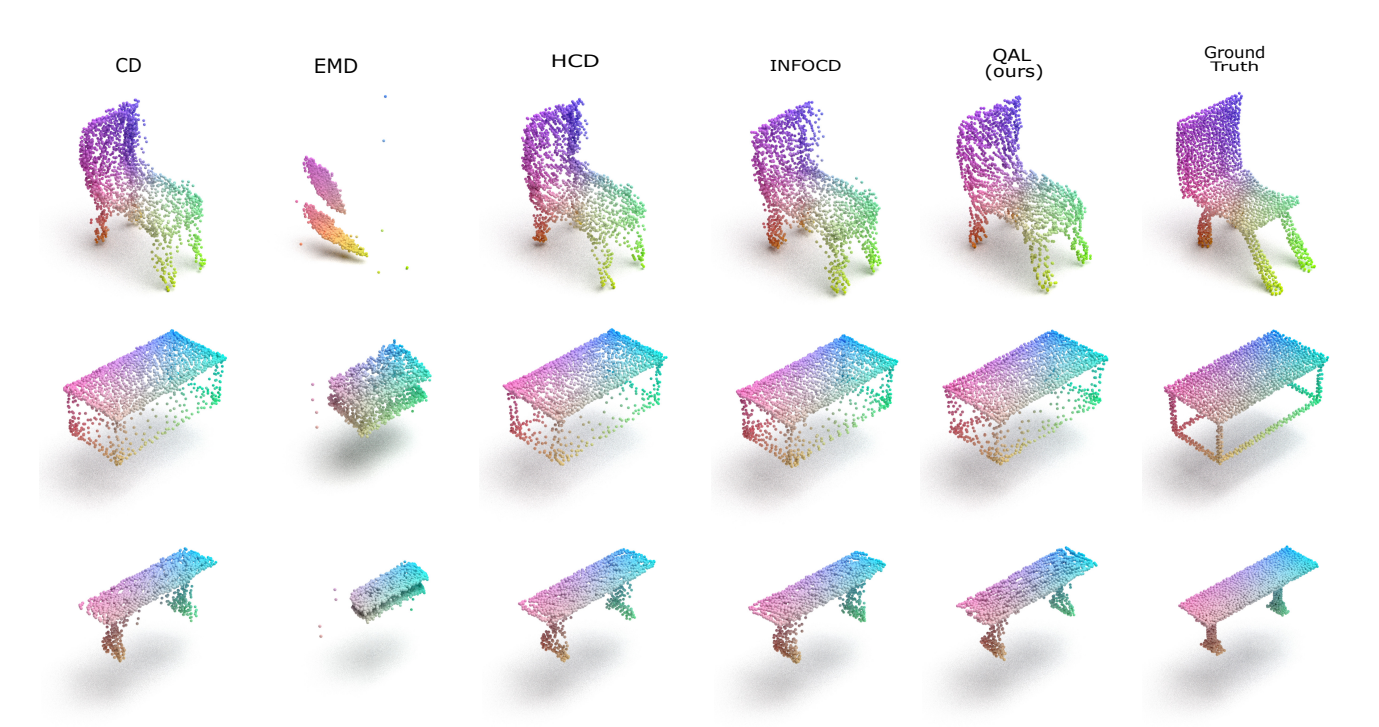


Figure 9. Representative reconstructions with PCN. CD and HCD reconstructions leave gaps in thin structures, while EMD collapses coverage with poor fidelity. InfoCD improves coverage modestly but introduces spurious clusters. QAL (ours) yields denser and more uniform point sets (+4.5 pts Cov. over CD), visibly recovering sharper chair backs and object contours. Input partial clouds are omitted for space; all methods use identical inputs.

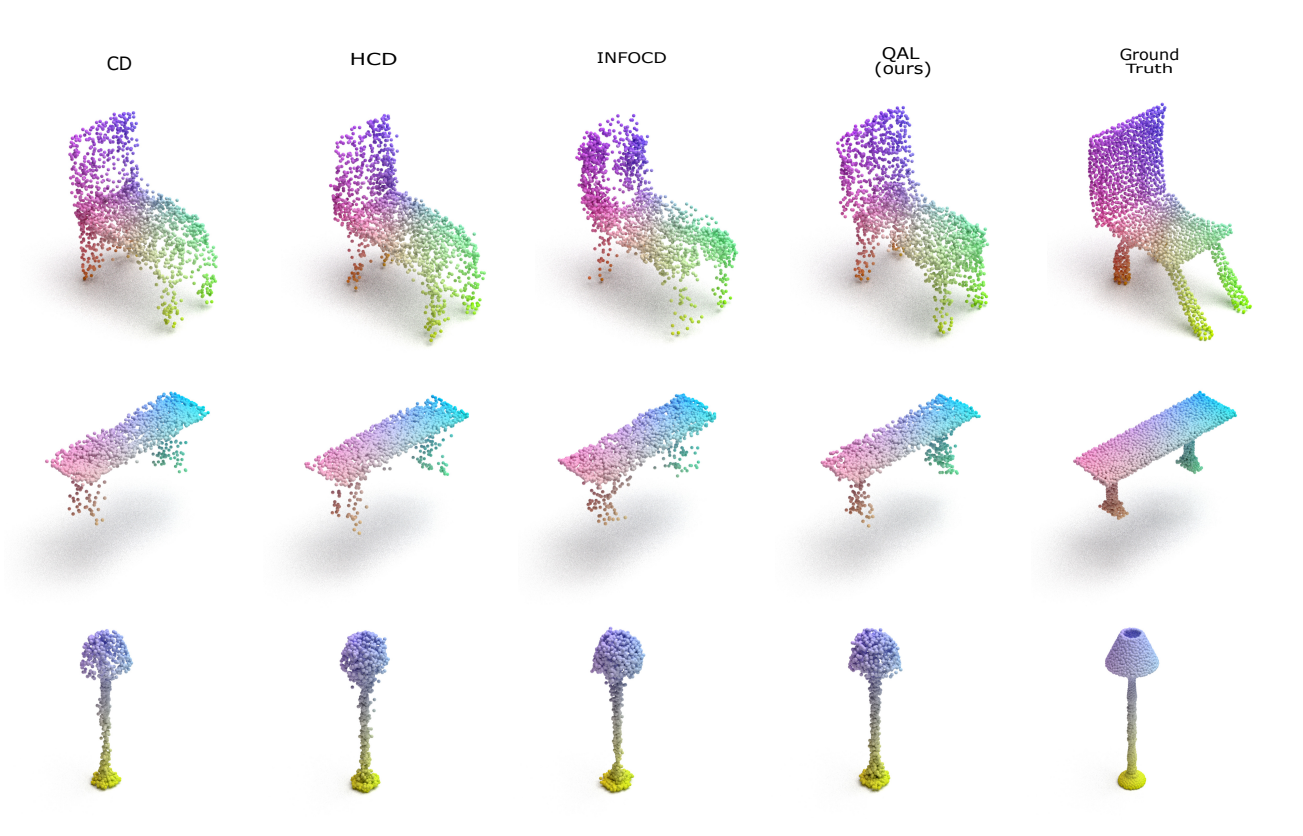


Figure 10. Representative reconstructions with TOPNet. CD, HCD, and InfoCD produce completions that look visually similar, consistent with flat CD/F1 values. However, QAL improves coverage (+4.3 pts Cov. over CD), filling in missing areas and producing more uniform reconstructions. These examples illustrate how CD/F1 miss improvements that are evident with coverage-aware evaluation. Input partial clouds are omitted for space; all methods use identical inputs.

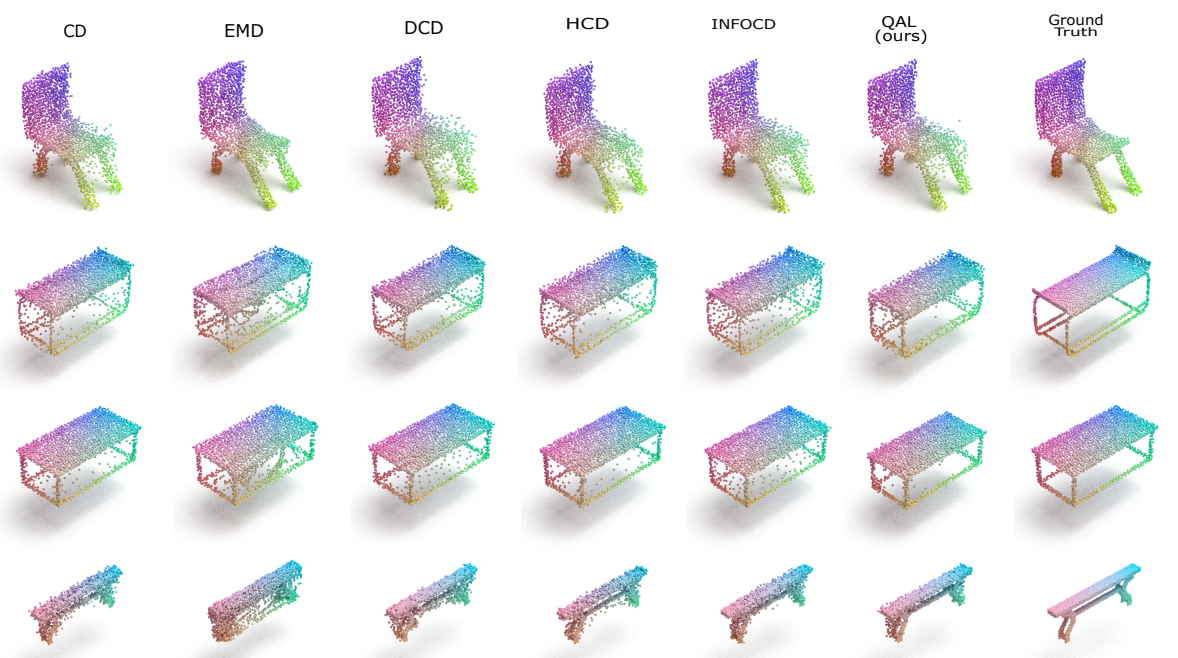


Figure 11. Representative reconstructions with ECG. CD and DCD achieve good overall alignment but leave subtle missing details. HCD and QAL both reach high coverage (91.6), yet CD differs (6.0 vs. 5.8), showing how CD alone can give misleading signals. Qualitatively, QAL better balances recall and precision, producing sharper and more consistent reconstructions without adding spurious points.

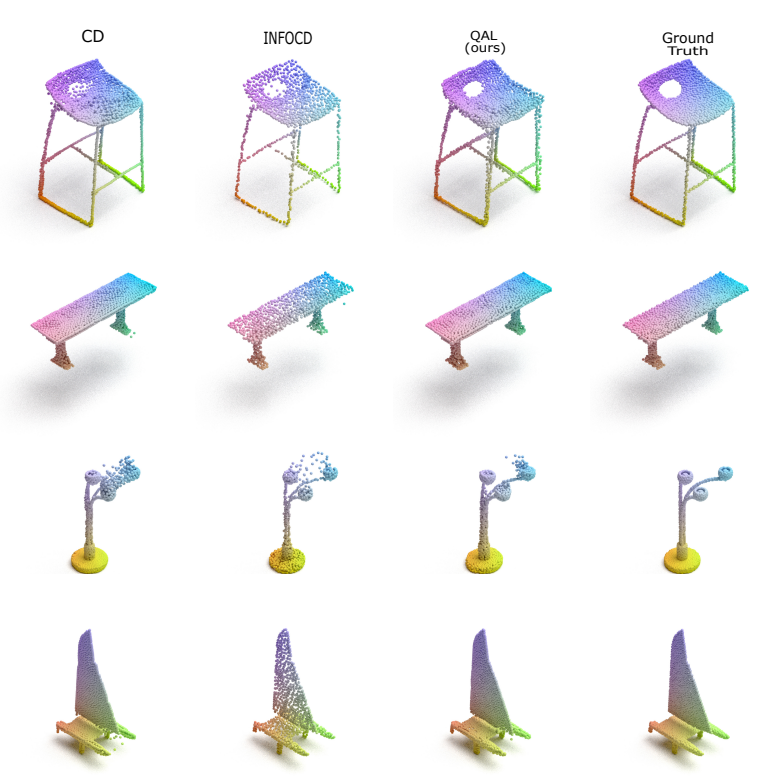


Figure 12. Representative reconstructions with SeedFormer. CD reconstructions miss fine chair details and introduce spurious points around thin lamp structures, while InfoCD collapses coverage (75.1) and clusters points densely in certain regions, leaving other areas sparse. In contrast, QAL restores coverage to 88.3 while maintaining balance between detail recovery and noise suppression, yielding more faithful reconstructions across both thin and coarse structures. Input partial clouds are omitted for space; all methods use identical inputs.